Journal of Drug Delivery Science and Technology 64 (2021) 102650

Contents lists available at ScienceDirect

Journal of Drug Delivery Science and Technology

journal homepage: www.elsevier.com/locate/jddst

Research paper

Smart GSH/pH dual-bioresponsive degradable nanosponges based on β-CD-appended hyper-cross-linked polymer for triggered intracellular anticancer drug delivery

Yutong Dai [a], Qingman Li [b], Shurong Zhang [a], Shan Shi [a], Yang Li [a], Xudong Zhao [a], Liping Zhou [a], Xin Wang [a], Yijian Zhu [a], Wei Li [a,*]

[a] Department of Medicinal Chemistry, School of Pharmacy, Chongqing Medical University, Chongqing, 400016, China
[b] The First Affiliated Hospital of Chongqing Medical University, Chongqing, 400016, China

ARTICLE INFO

Keywords:
Nanosponges
Dual-bioresponsive
β-Cyclodextrin
Controlled release
Hyper-cross-linked polymer

ABSTRACT

Efficient accumulation and on-demand intracellular drug release in the desired site are a crucial issue in developing ideal drug delivery systems (DDSs). Glutathione (GSH)/pH dual-bioresponsive degradable Nanosponges were developed based on β-CD-appended hyper-cross-linked polymer by one-pot polymerization of acryloyl-6- ethylenediamine-6-deoxy-β-Cyclodextrin (β-CD-NH-ACy), acrylic acid (AA) and *N*,*N*-bis(acryloyl)-cystamine (BACy) as cross-linker to deliver doxorubcin (DOX) and investigated for GSH/pH triggered DOX release, in which the massive carboxyl and amino groups, and disulfide bonds were used as pH and GSH bio-responsive fragments, respectively. In the proposed DDSs, DOX was readily incorporated into the three dimensional networks of the Nanosponges either as inclusion complexes or as non-inclusion complexes, with a high drug loading capacity of 22.6%. *In vitro* release studies suggested that the Nanosponges exhibited GSH/pH triggered disintegration and drug release performance, in which DOX release was significantly accelerated in acidic (pH5.0) and cytosolic reduction (10 mM GSH) conditions, with ~77.0% of DOX release. The morphology changes of DOX@Nanosponges in releasing media (pH5.0, 10 mM GSH) were further studied by TEM. Confocal microscopy observation demonstrated that DOX was delivered and released into cytoplasm and nucleus of A549 cells in 7 h incubation with DOX@Nanosponges. MTT assays manifested that the Nanosponges exhibited low cytotoxicity up to a concentration of 1000 μg/mL and DOX@Nanosponges had high anti-tumor activity. These findings demonstrated that the dual-bioresponsive Nanosponges may function as a promising platform for targeted delivery and intracellular drug controlled release in tumor therapy.

1. Introduction

Cancer has become one of the most dreaded diseases and the single most important barrier to increase life expectancy in both developing and developed countries [1]. Nowadays, the most common cancer treatment approaches are surgery, chemotherapy, radiation therapy and immunotherapy. Among them, surgery is the best treatment strategy for most solid tumors without metastasis. In spite of advances in surgical techniques, the residual tumor cells will increase the risk of cancer recurrence and metastasis [2]. The combination of chemotherapy and to a limited extent radiotherapy, has been the last resort to control cancer [3]. However, most of the conventional cancer chemotherapy is far from successful, mainly due to the lack of tumor selectivity of anticancer agents [4]. This situation is driving a rapid increase in the demand for developing the novel therapeutic strategies for effective cancer treatments, and the application of nanotechnology on cancer is anticipated to provide significant improvements in diagnosis and therapy of the disease. Therefore, tumor specific drug delivery systems (DDSs), which can selectively deliver anticancer drugs to the desired site by passive as well as active mechanisms and achieve controlled and predictable release of the drugs, have been intensely developed to improve the therapeutic efficacy of chemotherapeutics and simultaneously minimize the toxic side effects [5,6].

In the last decades, various DDSs including liposomes, polymer micelles, inorganic nanoparticles, viral vectors, dendrimers etc., have been explored for realizing tumor-selective delivery. Liposomes have often

* Corresponding author.
E-mail address: li_wei@cqmu.edu.cn (W. Li).

https://doi.org/10.1016/j.jddst.2021.102650
Received 8 December 2020; Received in revised form 31 May 2021; Accepted 3 June 2021
Available online 7 June 2021

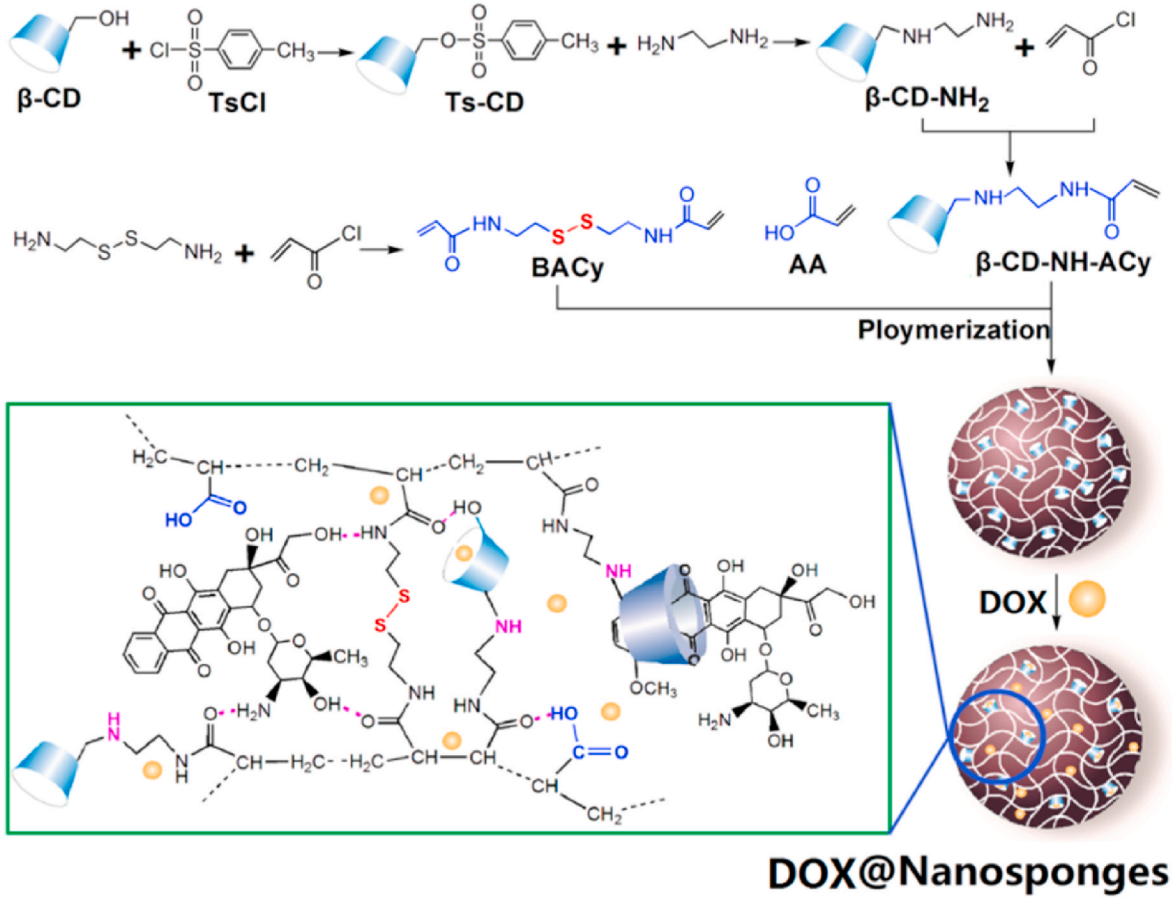

Scheme 1. Schematic illustration of the synthesis of Nanosponges and DOX@Nanosponges.

been used to deliver various drug modalities, but with relatively low efficiency and storage stability [7,8]. Inorganic nanoparticles, such as iron oxide, silica, gold, quantum dots, etc., are also attractive family of DDSs [9–11]. But they are non-biodegradable and difficult to load or conjugate with macromolecules. Polymeric micelles can fulfill the requirements for selective drug delivery [12], but in vivo instability, low cargo capacity and special storage conditions are problematic [13,14]. Viral vectors are effective for various active ingredients delivery as well as can be genetically or chemically conjugated to specific ligands to achieve tissue target, but have some issues such as easy of proteolytic degradation and potential safety concerns [15,16]. Dendrimers are employed for both the therapeutic and diagnostic applications [17], but it is difficulty in controlling the multi-step fabrication and purification process because numerous reaction steps take place at the same time in each growing step [18,19]. The above-mentioned strategies have shown promise, but other dosage forms using different strategies should also be developed for drastic improvements in the delivery of anticancer drug into the desired site.

Recently, a new type of cyclodextrin (CD) nano-vehicles are Nanosponges, which are composed of hyper-crosslinked α, β, and γ-CD polymers with porosity arising from CD nano-sized cavities and interconnecting voids, and possess innovative three dimensional (3D) mesh-like networks by chemical cross-linking [20–22]. Compared to CD, which can host various guest molecules with compatible geometry and polarity, Nanosponges are capable of entrapping and storing both hydrophilic and lipophilic small molecule drugs by 3D scaffolds or host-guest inclusion complex, and have been proposed as nanomedicine strategy to address challenging issues of DDSs, such as solubility, stability, sustained and controlled release [21,22], and even reduce the side effects of drugs [23]. Moreover, Nanosponges are also efficient carriers for proteins and other macromolecules, such as enzymes, DNA and oligonucleotides, which can increase the cellular internalization, prevent degradation and improve their bioavailability [20]. In the case of Nanosponges-loaded enzymes, their activity and efficiency are even enhanced in terms operative temperature and pH range [20]. Notably, Nanosponges are safe and biodegradable, display negligible toxicity on cell cultures, and are well-tolerated upon injection in experimental animals [24,25]. So Nanosponges are extensively used for delivering anticancer drugs [26], such as camptothecin [27], doxorubicin (DOX) [25,28], and paclitaxel [29]. Cytotoxicity studies suggested that camptothecin-loaded in Nanosponges was more than 20 times as effective than the drug alone and reduced by 70% the growth of prostate cancer cells in mouse xenograft models [27,30]. Furthermore, these Nanosponges can selectively extravasate in tumor tissue by the enhanced permeability and retention (EPR) effect, thereby achieving targeted delivery of drug inside the tumor tissue [28–30]. Although Nanosponges have already shown a great likelihood to be a targeting drug carrier for anti-cancer drugs, they have not yet been targeted to achieve controlled drug release to a desired cell or organ. pH and redox potential are often selected as pathological “triggers”, and used to develop new bio-responsive Nanosponges [24,27,31,32]. pH sensitive DDSs are usually designed to destabilize vehicles and release drugs in tumor tissues which the extracellular pH tends to be significantly more acidic (~ 6.5) than the pH of the blood (7.4), or in endosomal and lysosomal compartments with pH values typically as low as ~ 5.0, respectively [33]. In comparison, redox sensitive DDSs are developed with the aim to disassemble and release drugs in response to the intracellular glutathione (GSH) concentration, which is higher in tumor compared to normal tissue (approximately 0.5–10 mM vs. 2–20 μM) [33]. Significantly, chemoresistant cancer cells show even higher levels

of GSH [34]. Previous reports have demonstrated that drug-loaded GSH-Nanosponges exhibited remarkably higher effectiveness than the drug alone both in vitro and in vivo, and could escape the efflux drug pump, thus contributing to overcoming drug resistance [25,28]. Unfortunately, the Nanosponges still face some flaws including low loading capacity (only about 12%) [25,31], time consuming and complex synthetic procedures. Single-responsive DDSs can't yet completely meet demands of tumor-targeted delivery and controlled drug release to a desired cell or organ. Therefore, dual stimuli-bioresponsive DDSs will be a judicious choice for better anticancer therapy [35]. To the best of our knowledge, there are few reports on GDH/pH dual-bioresponsive Nanosponges based on β-CD as anticancer DDSs.

In the present work, we reported the one-step synthesis of a novel class of GSH/pH dual-bioresponsive degradable Nanosponges based on β-CD by the free radical inverse-emulsion polymerization of acryloyl-6-ethylenediamine-6-deoxy-β-CD and arcylic acid using *N*,*N*-bis(acryloyl) cystamine as a cross-linker (Scheme 1), which was fully characterized through physical-chemical data, drug loading and intracellular drug release behaviors in cancer cells. The particle size and morphology and the morphology changes of DDSs were tested by transmission electron microscopy (TEM). *In vitro* drug release behavior in response to different pH and GSH concentration, cell uptake, the cytotoxicity and anti-tumor activity were also investigated.

2. Materials and methods

2.1. Materials

Doxorubicin hydrochloride (DOX), acryloyl chloride, cystamine dihydrochloride, glutathione and *p*-toluenesulfonyl chloride were purchased from Aladdin Bio-Chem Technology Company (Shanghai, China). β-cyclodextrin, acrylic acid, Span-40, ammonium persulfate, 3-[4,5-dimethylthiazol-2-yl]-2,5-diphenyltetrazolium bromide (MTT) and ethylenediamine were obtained from Sigma-Aldrich (Shanghai, China). All other chemicals and reagents used were analytical grade.

2.2. Preparation of disulfide crosslinker N,N-bis(acryloyl)cystamine (BACy)

BACy was synthesized as previously described [36]. Typically, to a solution of cystamine·2HCl (2.82 g, 0.0125 mol) in deionized water (20 mL) was dropwise added a mixture solution of acryloyl chloride (2.26 g, 0.025 mol) in CH_2Cl_2 (3 mL) and NaOH (2.0 g, 0.05 mol) in deionized water (5 mL) under stirring at 0 °C over 1 h. After that, the reaction was allowed to proceed at room temperature for at least another 6 h. The product was extracted twice with CH_2Cl_2 and the organic layer was thoroughly dried with anhydrous Na_2SO_4. After remove of CH_2Cl_2 under vacuum, the resulting BACy was purified by recrystallization using 1/2 vol ratio of ethyl acetate/heptane as solvent.

2.3. Synthesis of 6-mono-(p-toluenesulfonyl)-β-cyclodextrin (Ts-CD)

Ts-CD was synthesized by the tosylation reaction of the C_6-hydroxyl groups of β-CD as described previously [37]. Briefly, in the reaction flask under N_2 atmosphere, to a stirred solution of NaOH (0.1 mol/L) in water (200 mL) was transferred β-CD (22.39 g, 19.70 mmol) at 0 °C in an ice bath until the β-CD was dissolved completely, followed by adding a solution of *p*-toluenesulfonyl chloride (TsCl, 5.51 g, 28.90 mmol) in acetonitrile (15 mL). The reaction mixture was stirred continuously for another 5 h under the same conditions. After remove of the unreacted TsCl by filtration, the filtrate was neutralized and then kept at 4 °C refrigerator for overnight. The Ts-CD was isolated as a white solid and dried under vacuum.

2.4. Synthesis of mono-(6-ethylenediamine-6-deoxy)-β-cyclodextrin (β-CD-NH_2)

In the reaction flask under N_2 atmosphere, 9 mL ethylenediamine was gradually added to the solution of Ts-CD (9.00 g 6.90 mmol) in dimethylformamide (30 mL) with stirring at 70 °C. The reaction was allowed to proceed for 7 h. Then acetone was added to precipitate the products. The solid was collected and dried under vacuum, obtaining β-CD-NH_2 as white powder.

2.5. Synthesis of acryloyl-6-ethylenediamine-6-deoxy-β-cyclodextrin (β-CD-NH- ACy)

Acryloyl chloride (1.75 g, 19.4 mmol) was added gradually to a solution of β-CD-NH_2 (2.23 g, 1.89 mmol) in 30 mL of $NaHCO_3$ solution with stirring in an ice bath under N_2 atmosphere. After that, the reaction was allowed to proceed for another 3 h. The white β-CD-NH_2-ACy was obtained by precipitation using acetone, and dried under vacuum.

2.6. Preparation of nanosponges

Nanosponges were prepared by the free radical inverse-emulsion polymerization as described elsewhere [38]. The continuous phase consists of toluene (w/w, 63%) and surfactant Span-40 (sorbitan monopalmitate, 2%), and the dispersed phase was composed of water (w/w, 34%) and various monomer including acrylic acid (AA, 672 mg, 9.330 mmol), β-CD-NH-ACy (580 mg, 0.473 mmol) and BACy (36.02 mg, 0.139 mmol). The dispersed phase was added dropwise to the continuous phase with ultrasonication for 10 min at 15 °C. The emulsion was purged with N_2 to remove the dissolved O_2 which otherwise can scavenge free radicals required for polymerization. Subsequently, the miniemulsion was heated to 40 °C, then the initiator ammonium persulfate (APS) and 1% **N,N,N′,N′**-Tetramethylethylenediamine (TEMED) were added and stirred for 5 h. After demulsification using ethanol, Nanosponges were isolated and washed for several times by centrifugation at 14, 000 rpm for 10 min. The collected Nanosponges were freeze-dried for 72 h to remove residual solvent.

2.7. Fabrication of DOX-loaded nanosponges (DOX@Nanosponges)

In order to load DOX in Nanosponges, to an aqueous suspension of Nanosponges (50 mg) in 30 mL water was added a solution of DOX (15 mg) dissolved in 10 mL phosphate buffer saline (PBS) and stirred for 24 h in the dark at room temperature. The aqueous suspension was then centrifuged at 18, 000 rpm for 20 min to separate the free drug. The DOX-loaded Nanosponges (DOX@Nanosponges) were stored at 4 °C until use. The concentration of DOX in the supernatant was determined by Shimadzu UV-2600 UV–Vis spectrophotometer at 480 nm [36] to calculate the drug loading capacity (DLC) and drug loading efficiency (DLE) by the following formula:

$$\text{DLC}\ (\%) = \frac{\text{initial weight of DOX} - \text{weight of DOX in supernatant}}{\text{weight of DOX@Nanosponges}} \times 100\%$$

$$\text{DLE}\ (\%) = \frac{\text{weight of DOX in Nanosponges}}{\text{initial weight of DOX}} \times 100\%$$

2.8. In vitro DOX release study

The in vitro release of DOX from DOX@Nanosponges was investigated at 37 °C under six different conditions, *i.e.* (i) PBS (100 mM, pH 7.4), (ii) PBS (100 mM, pH 6.5), (iii) acetate buffer (100 mM, pH 5.0), (iv) PBS containing 10 mM GSH (100 mM, pH 7.4), (v) PBS containing 10 mM GSH (100 mM, pH 6.5), and (vi) acetate buffer containing 10 mM GSH (100 mM, pH 5.0). DOX@Nanosponges suspension was divided

into six aliquots and immediately placed into dialysis tubes with a MWCO of 12000–14000. The dialysis tube was immersed into 50 mL of appropriate releasing medium and shaken at 120 rpm and 37 °C. At regular intervals, 5.0 mL of the receiving phase was withdrawn and replenished with an equal volume of fresh medium to maintain sink conditions. To avoid oxidation of GSH, the release media were perfused with N_2 [39]. DOX concentration was determined by UV–Vis spectrophotometer.

2.9. In vitro cytotoxicity assays

The cytotoxicity of free drug, empty and DOX@Nanosponges was studied by MTT assay using A549 cells. Cells were seeded in 96-well plates at a density of 1×10^4 cells per well and incubated in Dulbecco's modified Eagle's medium (DMEM) supplemented with 10% heat-inactivated fetal bovine serum (FBS) at 37 °C in a 5% CO_2 humidified environment for 24 h. The growth medium was removed and replaced by 180 μL of fresh DMEM medium. 20 μL of samples at different concentrations in PBS (10 mM, pH 7.4) were added. After 24, 48, and 72 h of incubation at 37 °C, the medium was aspirated and replenished with 100 μL of fresh medium, and 20 μL of MTT solution (5 mg/mL in DMEM) was added. The cells were incubated for another 4 h. After remover of the MTT solution, 150 μL of dimethylsulfoxide was added to dissolve the formed purple crystals. The absorbance was determined at 570 nm using a microplate reader (Bio-Rad, model 550). Untreated control cells were normalized to 100%. The relative cell viability was calculated by the following equation:

$$\text{Cell viablity } (\%) = \frac{OD_{sample} - OD_{blank}}{OD_{control} - OD_{blank}} \times 100\%$$

2.10. In vitro uptake study

A549 cells were seeded in confocal dishes and grown in DMEM medium containing 10% FBS overnight to make sure cells attached completely. The cells were incubated with prescribed amounts of free DOX or DOX@Nanosponges at 37 °C and 5% CO_2. After incubation for 1, 3, 5 and 7 h, the culture medium was removed. The cells were rinsed three times with PBS to remove the redundant DOX@Nanosponges, and then fixed with 4.0% formaldehyde at 37 °C for 10 min. The cell nuclei were stained by 4′,6-diamidino-2-phenylindole (DAPI) working solution for 10 min. Fluorescence images of cells were obtained with a Zeiss LSM 510 confocal laser scanning microscope (Carl Zeiss, Oberkochen, Germany).

2.11. Other instrumental methods

Fourier transform infrared spectroscopy (FT-IR) spectra of all samples were recorded on a PerkinElmer 1600 FTIR spectrometer (PerkinElmer, Italy) in the 4000-400 cm^{-1} range with a resolution of 4 cm^{-1}. The dried samples were mixed with KBr to be compressed to a plate for analysis. ^1H nuclear magnetic resonance (^1HNMR) spectra were recorded on Bruker 500 MHz NMR spectrometer (Bruker Avance, USA) with D_2O as solvent. Powder X-ray diffraction (XRD) analysis were recorded on XD-2 X-ray diffractometer persee (Beijing Persee instrument Co. Ltd, China) with Cu K_α radiation ($\lambda = 1.5405$ Å) operating at 30 kV voltage and 15 mA current density and using a scanning rate of 2°/min up to 50°. Transmission electron microscopy (TEM) micrographs were taken on a Hitachi 7500 electron microscope.

2.12. Statistical analysis

Data were displayed as mean ± S.D (standard deviation). Statistical data analyses were performed using one-way ANOVA (Origin Pro 9.0) for $n \geq 3$. The significant difference between the experimental and the control group was set at different levels as $p < 0.05$.

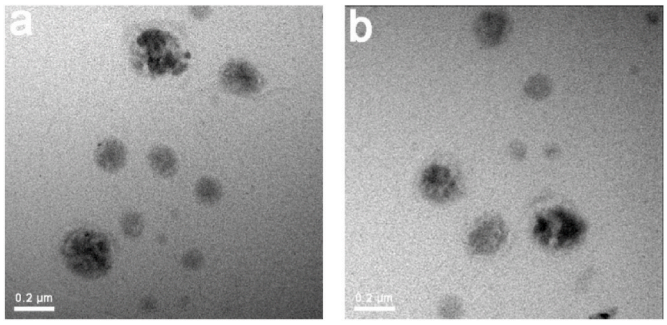

Fig. 1. TEM images of Nanosponges (a) and DOX@Nanosponges (b).

3. Results and discussion

3.1. Fabrication of the nanosponges

The purpose of the present study was to develop a novel one-pot synthesis approach to produce GSH/pH dual-bioresponsive Nanosponges and investigate their intracellular drug release behaviors in cancer cells. This one-pot procedure was based on the free radical inverse-emulsion polymerization of monomer β-CD-NH-ACy and AA in the presence of BACy cross-linker initiated by APS. The in-situ formation of Nanosponges based on β-CD-appended hyper-cross-linked polymer had 3D network structure (Scheme 1). Amino groups-containing β-CD-NH-ACy and carboxyl groups-containing AA as comonomer were used to impart the Nanosponges pH-responsiveness. Disulfide bond-containing BACy was utilized to endow the Nanosponges GSH-responsiveness, in which the disulfide bonds might be disintegrated in response to high intracellular GSH concentration while affording good stability in plasma with low GSH concentration [40]. The representative TEM image of the obtained Nanosponges (Fig. 1a) and DOX@Nanosponges (Fig. 1b) showed the spherical-like morphology. The average diameter of the DOX@Nanosponges (190 ± 20 nm) were slightly smaller than the blank ones (180 ± 23 nm), mainly owing to the encapsulated hydrophobic DOX molecules, which decreased their swelling degree in neutral aqueous media. The DLE and DLC were examined to be 90.3% and 22.56%, respectively. The DLC was higher than that of the previously reported GSH-responsive cyclodextrin-nanosponges (12 wt %) [25,31], and cyclodextrin-Calixarene Nanosponges (<20%) [32]. This may be ascribed to the combined interactions, including the 3D network providing the physical adsorption, the massive amino and carboxyl groups offering chemical adsorption by electrostatic interaction of hydrogen bond or slat bond, and β-CD forming inclusion complexes with DOX, etc.

3.2. Physicochemical characterization of nanosponges

The Nanosponges were first characterized by FTIR analysis. As can be seen in Fig. 2A, Nanosponges (curve c) showed typical β-CD absorption features of the ring vibrations at 578, 708, 756, and 943 cm^{-1}, the coupled C–O–C stretching/O–H bending vibrations at 1160 cm^{-1}, the coupled C–O/C–C stretching/O–H bending vibrations at 1035 and 1092 cm^{-1}, CH_2 stretching vibrations at 2917 cm^{-1}, C–H/O–H bending vibrations at 1415 $cm^{-1}$and O–H stretching vibrations at 3375 cm^{-1} [41,42]. This clearly confirmed that β-CD molecules were successfully introduced into the proposed DDSs. The signals at 1646 and 1560 cm^{-1} were attributed to the typical carbonyl group stretching vibration (amide I) and the *N*–H bending vibration (amide II) [36], while the peaks at 1075 cm^{-1} and 514 cm^{-1} were corresponded to -S-S- stretching vibration [40,43]. Furthermore, the signal at 1620 cm^{-1} (curve a and b) which was assigned to the C═C (sp2 carbon) stretching vibration disappeared [40,44], indicating that the free radical polymerization reaction took place. Additionally, the previously published reports had

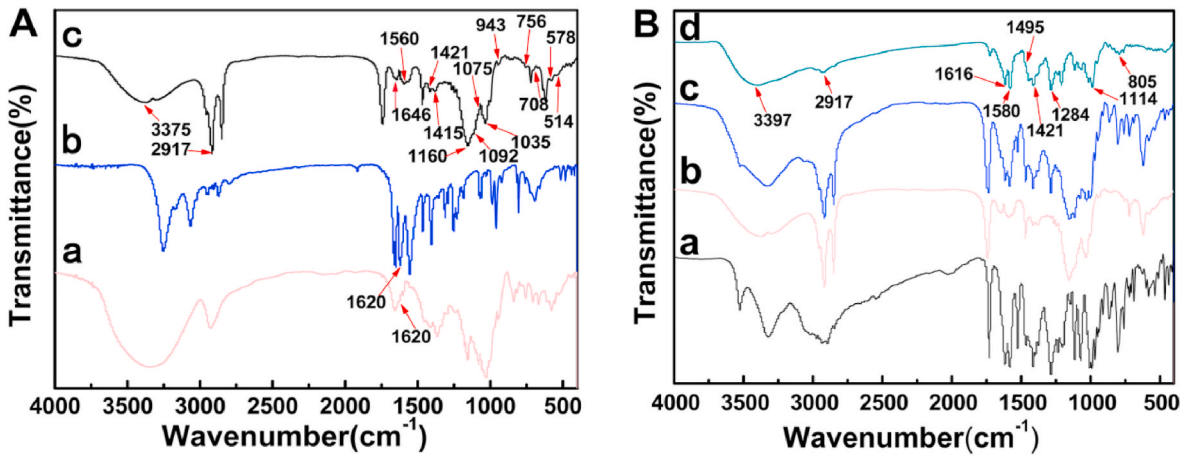

Fig. 2. FTIR spectra. A, β-CD-NH-ACy (a), BACy (b) and Nanosponges (c). B, free DOX (a), Nanosponges (b), physical mixture (c) and DOX@Nanosponges (d).

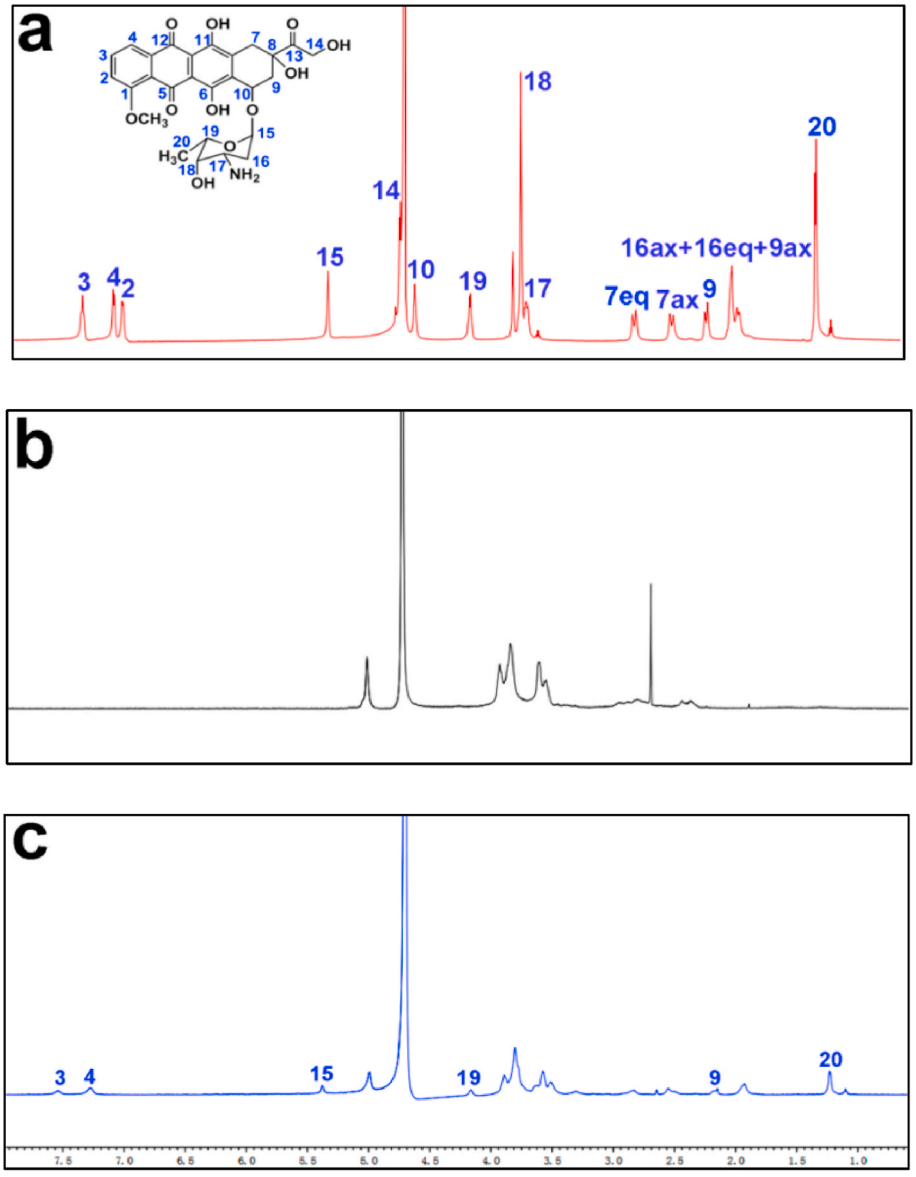

Fig. 3. [1]HNMR spectrums of free DOX (a), blank Nanosponges (b) and DOX@nanosponges (c).

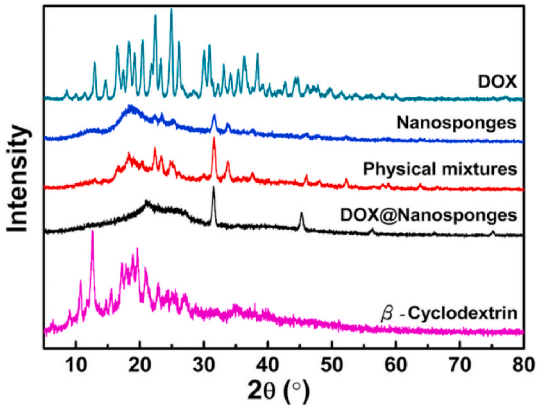

Fig. 4. The XRD diffractograms of free DOX, blank Nanosponges, physical mixtures of DOX and Nanosponges and DOX@Nanosponges.

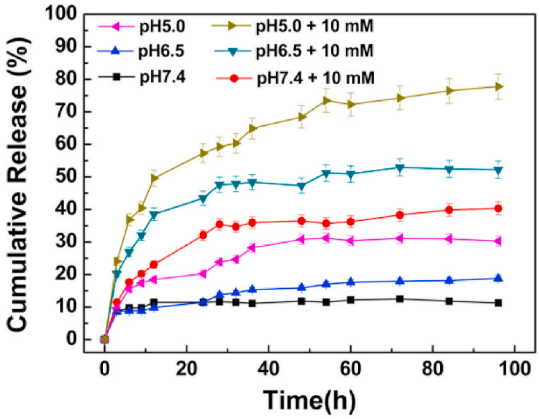

Fig. 5. The in vitro cumulative release profiles of DOX@Nanosponges at different pH values (7.4, 6.5 and 5.0) and different concentrations of GSH (0 and 10 mM).

demonstrated that multiple hydrogen bonds could be strong enough to fabricate a complex structure such as layer-by-layer assemblies and supramolecular dendrimers or D-networks [41,42,45]. Furthermore, when hydrogen bonding is formed, the O–H stretching vibration peak could exhibit typical red-shift [41,46]. Note that the O–H stretching vibration signal at 3375 cm^{-1} for Nanosponges (bonded OH mode) exhibited typical large red-shift compared with the free OH mode (located at about 3700 cm^{-1}), demonstrating that there existed a strong hydrogen bond between β-CD molecules and some O or *N*-containing groups of Nanosponges. The appearance of a new peak at about 1421 cm^{-1} clearly revealed the formation of intermolecular hydrogen bonds between the C═O groups and the *N*–H groups (C═O···H–N), owing to that the absorption peak is close to 1560 cm^{-1} (δNH) characteristic peak of the hydrogen bonded urethane groups [47]. These results indicated that the Nanosponges had been synthesized successfully by a free radical polymerization reaction. In addition, the FT-IR spectra of the DOX, blank Nanosponges, the physical mixture of DOX and Nanosponges, and DOX@nanosponges were shown in Fig. 2B. It was found that DOX (curve a) showed a series of characteristic peaks at 2917, 1616, 1580, 1495, 1284, 1114 and 805 cm^{-1} [48], and the physical mixture spectrum (curve c) was expected to be the sum of the DOX (curve a) and Nanosponges (curve b). Compared with DOX and the physical mixture, for DOX@nanosponges (curve d) there were significant changes in the characteristic absorption peaks of DOX; some signals disappeared and some signals became less intense, particularly in the range of 1616–1495 cm^{-1} for DOX aromatic rings and 1284-805 cm^{-1}, but it retained all characteristic peaks from Nanosponges. The complete disappearance or strong reduction of the DOX characteristic bands was owing to the change in environment after the formation of the host-guest complexes between DOX and β-CD or supramolecular encapsulation between DOX and carrier networks. In addition, the global shape of the broad peak at 3397 cm^{-1} for –OH group (curve d) was modified leading to a decrease of the half-band width and the new peak at about 1421 cm^{-1} appeared when DOX loading occurred, revealing the formation of intermolecular hydrogen bonds between DOX and carrier network (Scheme 1). These strong interactions between DOX and Nanosponges could be further demonstrated by the following ^{1}HNMR analysis. The ^{1}HNMR spectra of free DOX (Fig. 3a) and blank Nanosponges (Fig. 3b) clearly exhibited a series of characteristic peaks. For DOX, all of characteristic signals were attributed to the corresponding protons in the DOX molecule [49]. However, for DOX@Nanosponges, it was noticed that the H signals from ~7.1 to 7.7, at about 5.4, 4.15, 2.1 and 1.2 ppm which were assigned to No. 3 and 4, 15, 19, 9 and 20 protons' peak of DOX became weak (Fig. 3c), implying that DOX was efficiently loaded into Nanosponges.

P-XRD is a very useful technique to investigate the structural arrangement within DDSs because the structural arrangement of inside the molecule would interfere with drug encapsulation and release behaviors. Crystalline intense peaks of β-CD at 2θ of 4.7°, 9.1°, 10.7°, 11.8°, 14.9°, 17.2°, 19.8° and 23° [50] were not seen in the XRD pattern of Nanosponges (Fig. 4), demonstrating that crystal structure of β-CD was converted into amorphous owing to the polymerization reaction and β-CD molecules distributed homogenously in Nanosponges without the formation phase-separated crystal aggregates. While characteristic intense signals of DOX were observed at 2θ of 12.35°, 16.44°, 18.76°, 20.46°, 22.50°, 24.94°, 26.14° and 30.06°, indicative of crystalline structure. As expected, the diffractogram of the physical mixture did not reveal any deviation in the peak position with respect to those of DOX and Nanosponges. Notably, after loading of crystalline DOX molecules into amorphous Nanosponges, the signals corresponded to the DOX were not observed in the XRD pattern of DOX@Nanosponges, which clearly supported that DOX was an amorphous phase in Nanosponges and formed the inclusion complex with β-CD. Consequently, it could also be concluded that β-CD-appended hyper-cross-linked polymer was formed. The appearance of new lines at 2θ of 45.10° and 56.25° may be due to the presence of new solid crystalline phases which corresponded to a host-guest complexes of the same nature [51].

3.3. *In vitro DOX release and morphological changes of the Nanosponges*

Controlled release of DOX in the acidic/redox environments of the tumor is important to reduce side effect and enhance the drug bioavailability. The in vitro release of DOX from DOX@Nanosponges was investigated at 37 °C under six different conditions, including (i) PBS (100 mM, pH 7.4), (ii) PBS (100 mM, pH 6.5), (iii) acetate buffer (100 mM, pH 5.0), (iv) PBS containing 10 mM GSH (100 mM, pH 7.4), (v) PBS containing 10 mM GSH (100 mM, pH 6.5), and (vi) acetate buffer containing 10 mM GSH (100 mM, pH 5.0). There was no obvious burst drug release in the six drug release profiles (Fig. 5). At physiological pH (pH7.4) about 11.0% of DOX originally encapsulated within Nanosponges was released, even after 96 h incubation. When pH reduced to 6.5 and 5.0 mimicking the tumor extracellular and intracellular microenvironment (endosomal compartments [34], about 19.0% and 31.0% of DOX was released in 96 h, respectively. Obviously, the drug release ratio at the acidic medium was much higher than that in the physiological medium, demonstrating the pH-triggered drug release property. This phenomenon can be explained by these facts. At neutral pH7.4, the ionized amino group of DOX (pKa of 8.3 [52] and β-CD-NH-ACy units (-NH_3^+) and the deprotonated carboxyl group of AA units (-COO^-) were combined tightly by electrostatic interaction, leading to the low release of DOX [53,54]. While on reaching acidic environments (especially pH5.0), most of the carboxyl groups of AA units were in a non-ionized state (-COOH) and became hydrophobic [54], and the

Table 1
Fitted DOX release parameters with Korsmeyer-Peppas and Higuchi models.

Releasing media	Korsmeyer-Peppas		Higuchi	
	n	R^2	*k*	R^2
pH7.4	0.08233	0.73772	0.75334	0.47029
pH7.4 + 10 mM GSH	0.34547	0.91844	3.88594	0.86332
pH6.5	0.27232	0.93199	1.72083	0.91895
pH6.5 + 10 mM GSH	0.26546	0.90860	4.75039	0.80858
pH5.0	0.32405	0.92956	3.05392	0.88101
pH5.0 + 10 mM GSH	0.31655	0.95435	7.33992	0.90372

amino groups of β-CD-NH-ACy units and DOX were in a protonated state **($-NH_3^+$)**, which destroyed the interaction (electrostatic interaction or hydrogen bond) between DOX and the Nanosponges in DDSs, caused the internal mutual strong exclusion between the Nanosponges and DOX leading to DOX@Nanosponges swell and more of the incorporated DOX release [53,54]. Furthermore, a positive charge was attained by accepting protons thereby promoting cell uptake of the DOX@Nanosponges. On the other hand, as for the pH-responsive Nanosponges, the premature drug leakage at pH7.4 was about 11.0%, and a release ratio of 19.0% was obtained at pH6.5 because of its excellent responsiveness in the desired pH range, implying that the DOX@Nanosponges could effectively accommodate DOX before entering cancer cells. The character of the minimal drug leakage from the DOX@Nanosponges would be of great significance for practical applications due to the low side effects to normal tissues. The cumulative release was further boosted in presence of 10 mM GSH (equal to the concentration of GSH intra the cancer cells) [34] at pH7.4, 6.5 and 5.0, with ~40.0%, ~52.0% and ~77.0% of DOX released in 96 h, respectively, much higher than these values without GSH, indicating the excellent reduction responsive triggered drug release performance of the DOX@Nanosponges. In the stimulated tumor intracellular microenvironment (pH5.0 and 10 mM GSH), the disulfide bonds cleavage-induced the 3D worknets breakage and lower pH-induced swelling of the DOX@Nanosponges resulted in that the Nanosponges were disintegrated into water soluble fragments, triggering the DOX rapid dissociation and release from the network structure of Nanosponges, simultaneously accompanied by release of DOX from the cavities of β-CD. The drug release mechanism was also simulated with Korsmeyer-Peppas (Fig. S1) and Higuchi (Fig. S2) models, and the values of release exponent (*n*), kinetic constant (*k*) and regression coefficient (R^2) were summarized in Table 1. R^2 was often used as criteria to evaluate the accuracy of these models. According to the obtained R^2 values the Korsmeyer-Peppas kinetic model exhibited a better fit for the DOX release from DOX@Nanosponges, suggesting the drug release mechanism could be better described with the Korsmeyer-Peppas models, The *n* value from Korsmeyer-Peppas model, consist of $0.5 < n < 1.0$ for mass transfer following non-Fickian or anomalous diffusion model and $n \leq 0.5$ for Fickian diffusion mechanism. The *n* values were less than 0.5 and Fickian diffusion was observed for DOX release period. As for the Higuchi model, all the *k* values were near or higher than 1, implying the drug release mechanism was governed by Fickian diffusion. Even so, the DOX release from the Nanosponges was very complicated and difficult to understand thoroughly.

The incorporation of bioreducible disulfide bonds into the Nanosponges is expected to improve the biodegradation behavior of DDSs. The morphological changes of Nanosponges during the course of DOX release in releasing medium at pH 5.0 with 10 mM GSH were directly observed by TEM. Obviously, the drug release process was characterized by swelling and disintegration of the Nanosponges (Fig. 6). Compared with the initial DOX@Nanosponges, the spherical Nanosponges became irregular and loose after 12 h of incubation (Fig. 6b), and the compact structure of 3D networks begin to disintegrate (Fig. 6c). With the increase in the incubation time, the degree of disintegration of the Nanosponges gradually increased over the next 72 h. By 96 h of incubation, almost all of the Nanosponges were collapsed into small stripe fragments (Fig. 6g). Interestingly, even up to 96 h of incubation, there were still a few of Nanosponges which did not completely disintegrated into fragments (Fig. 6h). This provided the favorable conditions for drug

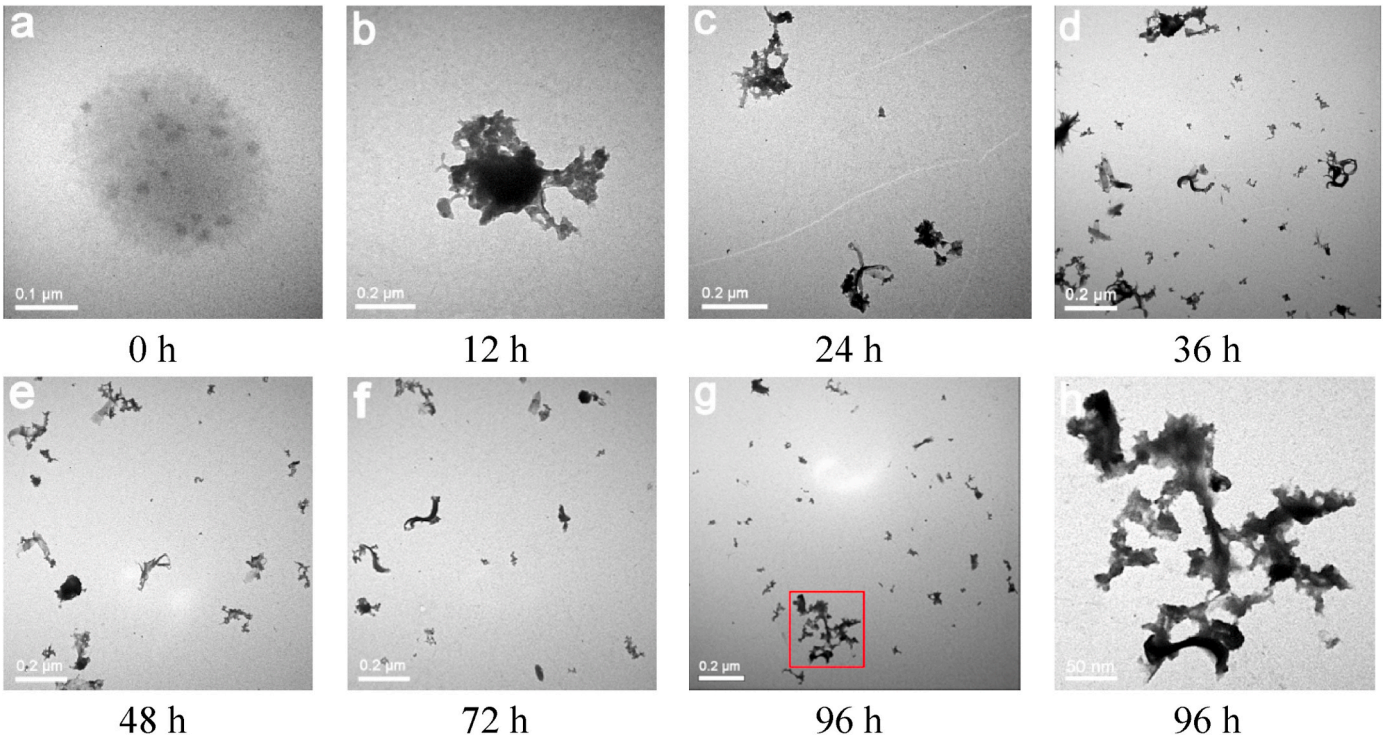

Fig. 6. TEM images depicting the morphology of DOX@Nanosponges in releasing media at pH5.0 with 10 mM GSH, (a) images of initial DOX@Nanosponges before incubation, (b), 12 h, (c), 24 h, (d), 36 h, (e), 48 h, (f) 72 h and (g) 96 h of incubation, respectively. (h) the higher magnification of the red boxed section in image (g). (For interpretation of the references to colour in this figure legend, the reader is referred to the Web version of this article.)

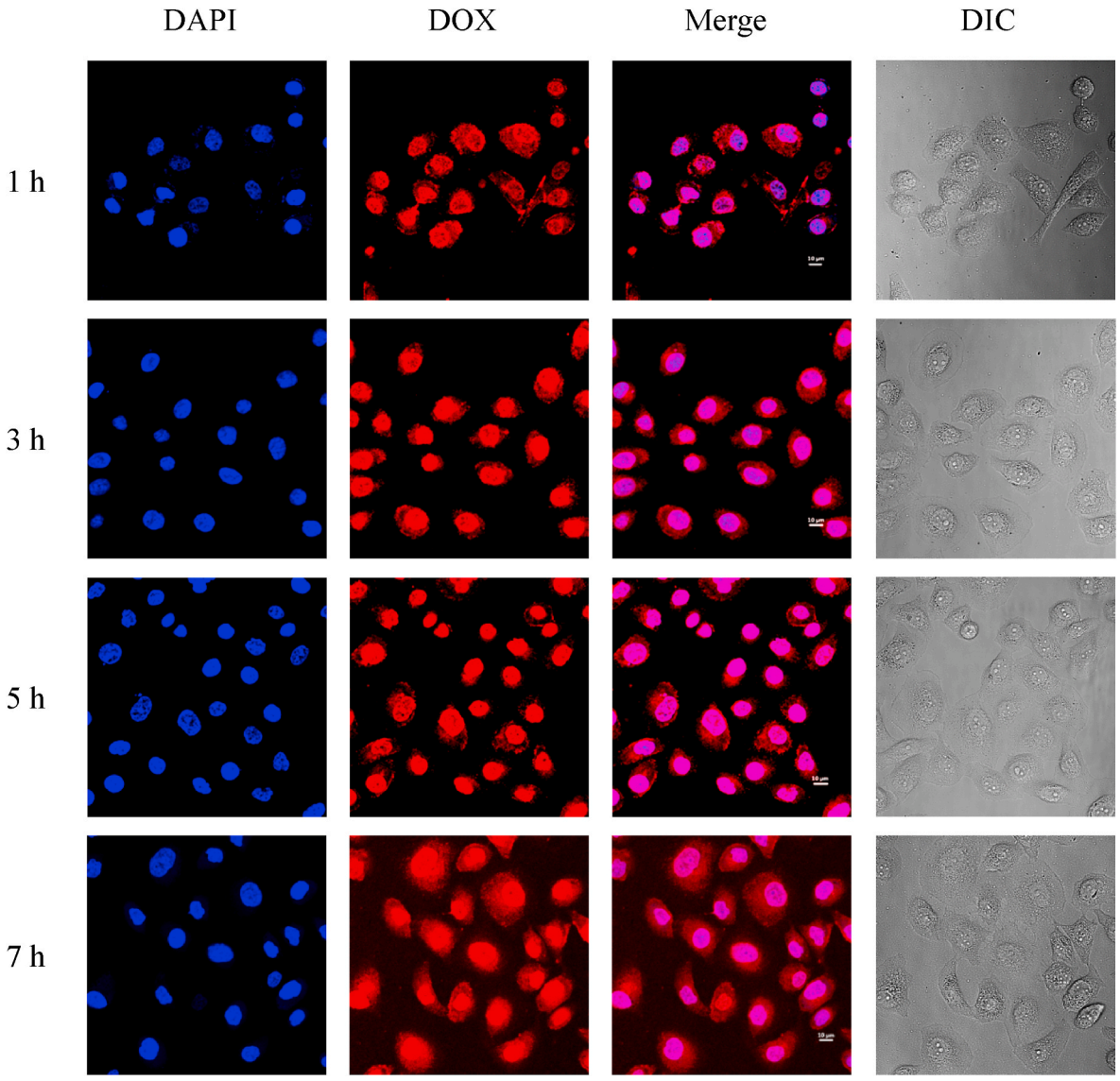

Fig. 7. CLSM images of A549 cells after incubation with DOX@Nanosponges (10 mg DOX equiv/mL) for 1 h, 3 h, 5 h and 7 h, respectively. Scale bar: 10 μm.

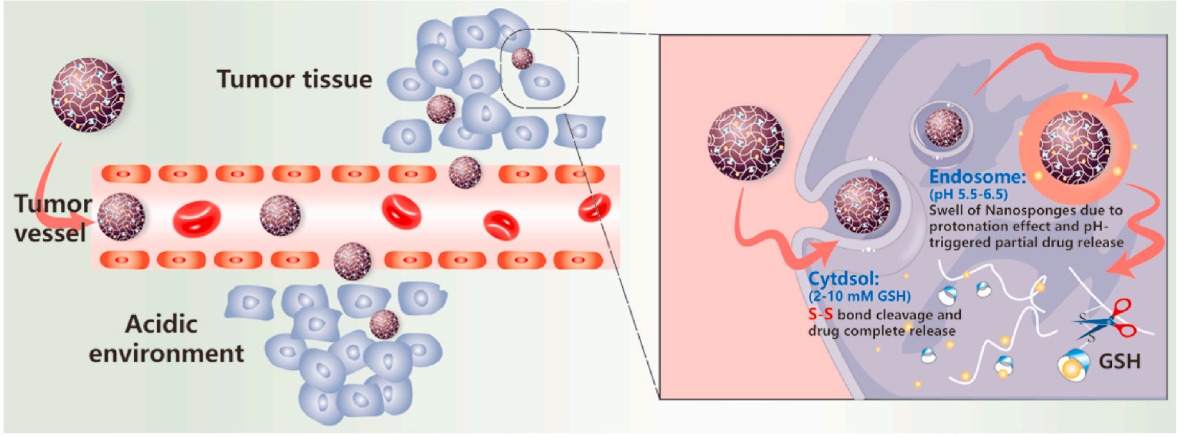

Scheme 2. Illustration of pH/GSH dual-bioresponsive degradable Nanosponges for dually activated intracellular release of DOX.

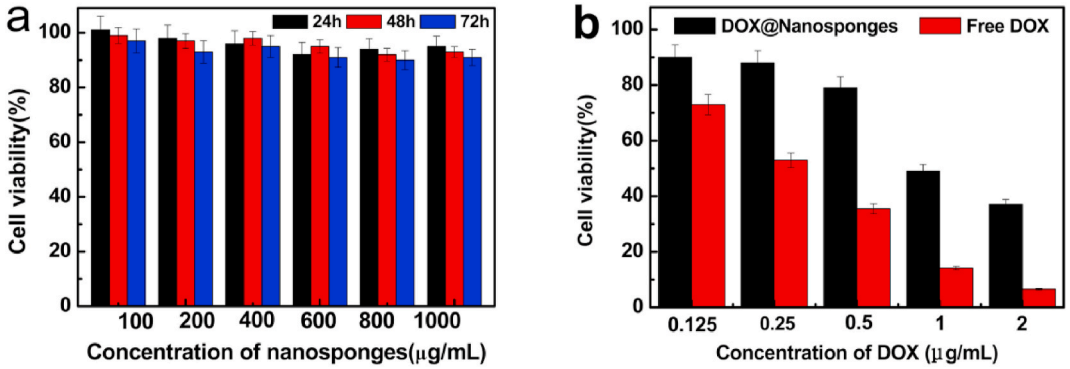

Fig. 8. (a) Viabilities of A549 cells treated with Nanosponges for 24, 48 and 72 h, respectively, (b) DOX@Nanosponges and free DOX for 72 h.

sustained and controlled release.

3.4. Uptake and intracellular DOX release

The uptake of DOX into the tumor cell nucleus is crucial because DOX has to intercalate with DNA to kill the tumor cells [39]. A549 cells treated with DOX@Nanosponges were observed by CLSM to visualize cellular uptake and track the intracellular localization and drug release profiles. For the experiment, A549 cells were stained with DAPI to locate the nucleus (blue) while DOX presented red fluorescence. A549 cells were incubated for 1, 3, 5 and 7 h with DOX@Nanosponge. CLSM observation was carried out to observe the combination of the red fluorescence (DOX) and the blue fluorescence (DAPI) to confirm whether the drugs enter the nucleus. As can be seen from Fig. 7, strong DOX fluorescence was observed in the cell cytoplasm and a relatively weak red fluorescence presented in the cell nucleus following 1 h incubation with DOX@Nanosponges. However, the red fluorescence intensity inside the cell nuclei increased gradually with the increase in incubation time and reached a maximum at 7 h. It was proved that the DOX@Nanosponges were internalized into the tumor cells by endocytosis. Upon endocytosis, the DOX@Nanosponges were swollen due to the protonation effect resulting in partial DOX release in endosomes, and then the swollen Nanosponges escaped form endosomes following further trafficking to cytoplasm where Nanosponges would rapidly disintegrate due to disulfide bonds cleavage and DOX was completely released in response to high intracellular GSH concentration (Scheme 2), simultaneously accompanied by DOX release from the cavities of β-CD. The released DOX was finally translocated to nucleus to exert cytotoxicity against tumor cells.

3.5. Antitumor activity analysis

To determine the antitumor activity of the DOX@Nanosponges, A549 cells were treated with different concentrations of DOX@Nanosponges, blank ones and free DOX for 72 h, and cell viability was evaluated by MTT assay. It was found that the Nanosponges was practically non-toxic (cell viabilities $>$ 90%) up to a tested concentration of 1000 μg/mL in 72 h (Fig. 8a), confirming that the Nanosponges had good biocompatibility. DOX@Nanosponges, however, exhibited significant antitumor activity against A549 cells following 72 h incubation (Fig. 8b). The half maximal inhibitory concentration (IC_{50}) of DOX@Nanosponges was 1.201 μg DOX equiv/mL for A549 cells, which was much higher than that of reported DOX-loaded degradable block copolymer (27 μg/mL [55], 15 μg/mL [56] and 3.2 μg/mL [57]. This greater inhibitory effect of DOX@Nanosponges was in agreement with the CLSM observations that Nanosponges mediated fast targeted intracellular drug release by intracellular reduction in the acid environment to directly bind to the nucleus, thereby preventing loss of the DOX and enhancing the antitumor activity.

4. Conclusions

We have demonstrated that the GSH/pH dual-bioresponsive degradable Nanosponges based on β-CD-appended hyper-cross-linked polymer efficiently deliver doxorubicin into tumor cells and respond to endosomal pH as well as cytoplasmic GSH to enhance intracellular doxorubicin release, leading to the improved anti-tumor activity. The smart Nanosponges exhibit several interesting characteristics including low degradable and cytotoxicity; decent drug loading capacity; sufficiently stable with low drug release (only 11% doxorubicin release in 96 h) under physiological conditions (pH7.4, 37 °C); and fast and maximum drug release triggered by acidic endosomal pH and cytoplasmic GSH so on. All these characteristics demonstrate that the GSH/pH dual-bioresponsive degradable Nanosponges can be employed as a potential anticancer delivery system for future applications in cancer chemotherapy.

Declaration of competing interest

The authors declare no competing financial interest.

Acknowledgment

The authors acknowledge the financial support from Chongqing Municipality Education Commission (KJ1400212), the Municipal Science and Technology Committee of Chongqing (CSTC2014jcy-jA0019), and School of Pharmacy, Chongqing Medical University.

Appendix A. Supplementary data

Supplementary data to this article can be found online at https://doi.org/10.1016/j.jddst.2021.102650.

Author statement

Yutong Dai: Methodology, Investigation, Data curation, Writing-original draft. Qingman Li: Methodology, Investigation, Writing-original draft. Shurong Zhang: Methodology, Investigation, Writing-original draft. Shan Shi: Investigation. Yang Li: Investigation. Xudong Zhao: Liping Zhou, Investigation. Xin Wang: Supervision. Yijian Zhu: Supervision. Wei Li: Conceptualization, Writing - review & editing, Project administration, Funding acquisition.

References

[1] F. Bray, J. Ferlay, I. Soerjomataram, R.L. Siegel, L.A. Torre, A.I. Jemal, Global cancer statistics 2018: GLOBOCAN estimates of incidence and mortality worldwide for 36 cancers in 185 countries, CA A Cancer J. Clin. 68 (2018) 394–424.
[2] A.N. Tavare, N.J. Perry, L.L. Benzonana, M. Takata, D. Ma, Cancer recurrence after surgery: direct and indirect effects of anesthetic agents, Int. J. Canc. 130 (2012) 1237–1250.

[3] A.J. Breugom, M. Swets, J.F. Bosset, L. Collette, A. Sainato, L. Cionini, et al., Adjuvant chemotherapy after preoperative (chemo) radiotherapy and surgery for patients with rectal cancer: a systematic review and meta-analysis of individual patient data, Lancet Oncol. 16 (2015) 200–207.

[4] K.S. Albain, R.S. Swann, V.W. Rusch, A.T. Turrisi, F.A. Shepherd, C. Smith, et al., Radiotherapy plus chemotherapy with or without surgical resection for stage III non-small-cell lung cancer: a phase III randomised controlled trial, Lancet 374 (2009) 379–386.

[5] T.M. Allen, P.R. Cullis, Drug delivery systems: entering the mainstream, Science 303 (2004) 1818–1822.

[6] M.E. Davis, Z. Chen, D. Shin, Nanoparticle therapeutics: an emerging treatment modality for cancer, Nat. Rev. Drug Discov. 7 (2008) 771–782.

[7] N. Filipczak, J. Pan, S.S.K. Yalamarty, V.P. Torchilin, Recent advancements in liposome technology, Adv. Drug Deliv. Rev. 156 (2020) 4–22.

[8] S. Shah, V. Dhawan, R. Holm, M.S. Nagarsenker, Y. Perrie, Liposomes: advancements and innovation in the manufacturing process, Adv. Drug Deliv. Rev. 154–155 (2020) 102–122.

[9] M.I. Setyawati, D.T. Leong, Mesoporous silica nanoparticles as an antitumoral-angiogenesis strategy, ACS Appl. Mater. Interfaces 9 (2017) 6690–6703.

[10] L.H. Reddy, J.L. Arias, J. Nicolas, P. Couvreur, Magnetic nanoparticles: design and characterization, toxicity and biocompatibility, pharmaceutical and biomedical applications, Chem. Rev. 112 (2012) 5818–5878.

[11] E.C. Dreaden, A.M. Alkilany, X. Huang, C.J. Murphy, M.A. El-Sayed, The golden age: gold nanoparticles for biomedicine, Chem. Soc. Rev. 41 (2012) 2740–2779.

[12] A.S. Deshmukh, P.N. Chauhan, M.N. Noolvi, K. Chaturvedi, K. Ganguly, S. S. Shukla, et al., Polymeric micelles: basic research to clinical practice, Int. J. Pharm. 532 (2017) 249–268.

[13] C.J.F. Rijcken, O. Soga, W.E. Hennink, C.F. van Nostrum, Triggered destabilisation of polymeric micelles and vesicles by changing polymers polarity: an attractive tool for drug delivery, J. Contr. Release 120 (2007) 131–148.

[14] H. Xu, Q. Yao, C. Cai, J. Gou, Y. Zhang, H. Zhong, et al., Amphiphilic poly(amino acid) based micelles applied to drug delivery: the in vitro and in vivo challenges and the corresponding potential strategies, J. Contr. Release 199 (2015) 84–97.

[15] Y.H. Chung, H. Cai, N.F. Steinmetz, Viral nanoparticles for drug delivery, imaging, immunotherapy, and theranostic applications, Adv. Drug Deliv. Rev. 156 (2020) 214–235.

[16] H. Fu, D.M. McCarty, Crossing the blood-brain-barrier with viral vectors, Curr. Opin. Virol. 21 (2016) 87–92.

[17] A.R. Menjoge, R.M. Kannan, D.A. Tomalia, Dendrimer-based drug and imaging conjugates: design considerations for nanomedical applications, Drug Discov. Today 15 (2010) 171–185.

[18] L.M. Bronstein, Z.B. Shifrina, Dendrimers as encapsulating, stabilizing, or directing agents for inorganic nanoparticles, Chem. Rev. 111 (2011) 5301–5344.

[19] M.A. Quadir, R. Haag, Biofunctional nanosystems based on dendritic polymers, J. Contr. Release 161 (2012) 484–495.

[20] V. Venuti, B. Rossi, A. Mele, L. Melone, C. Punta, D. Majolino, C. Masciovecchio, F. Caldera, F. Trotta, Tuning structural parameters for the optimization of drug delivery performance of cyclodextrin-based nanosponges, Expet Opin. Drug Deliv. 14 (2017) 331–340.

[21] S. Pawar, P. Shende, F. Trotta, Diversity of β-cyclodextrin-based nanosponges for transformation of actives, Int. J. Pharm. 565 (2019) 333–350.

[22] A. Jain, S.K. Prajapati, A. Kumari, N. Mody, M. Bajpai, Engineered nanosponges as versatile biodegradable carriers: an insight, J. Drug Deliv. Sci. Technol. 57 (2020), 101643.

[23] D. Zhang, P. Lv, C. Zhou, Y. Zhao, X. Liao, Bo Yang, Cyclodextrin-based delivery systems for cancer treatment, Mat. Sci. Eng. C-Mater. 96 (2019) 872–886.

[24] P. Shende, Y.A. Kulkarni, R.S. Gaud, K. Deshmukh, R. Cavalli, F. Trotta, F. Caldera, Acute and repeated dose toxicity studies of different β-cyclodextrin-based nanosponge formulations, J. Pharm. Sci. 104 (2015) 1856–1863.

[25] M. Daga, I.A.M. de Graaf, M. Argenziano, A.S.M. Barranco, M. Loeck, Y. Al-Adwi, et al., Glutathione-responsive cyclodextrin-nanosponges as drug delivery systems for doxorubicin: evaluation of toxicity and transport mechanisms in the liver, Toxicol. Vitro 65 (2020), 104800.

[26] F. Trotta, C. Dianzani, F. Caldera, B. Mognetti, R. Cavalli, The application of nanosponges to cancer drug delivery, Expet Opin. Drug Deliv. 11 (2014) 931–941.

[27] R. Minelli, R. Cavalli, L. Ellis, P. Pettazzoni, F. Trotta, E. Ciamporcero, et al., Nanosponge- encapsulated camptothecin exerts anti-tumor activity in human prostate cancer cells, Eur. J. Pharmaceut. Sci. 47 (2012) 686–694.

[28] M. Daga, C. Ullio, M. Argenziano, C. Dianzani, R. Cavalli, F. Trotta, et al., GSH-targeted nanosponges increase doxorubicin-induced toxicity "in vitro" and "in vivo" in cancer cells with high antioxidant defenses, Free Radic. Biol. Med. 97 (2016) 24–37.

[29] R. Namgung, Y.M. Lee, J. Kim, Y. Jang, B.H. Lee, I.S. Kim, et al., Poly-cyclodextrin and poly-paclitaxel nano-assembly for anticancer therapy, Nat. Commun. 5 (2014) 3702.

[30] C.L. Gigliotti, R. Minelli, R. Cavalli, S. Occhipinti, G. Barrera, S. Pizzimenti, et al., In vitro and in vivo Therapeutic evaluation of camptothecin-encapsulated β-cyclodextrin nanosponges in prostate cancer, J. Biomed. Nanotechnol. 12 (2016) 114–127.

[31] F. Trotta, F. Caldera, C. Dianzani, M. Argenziano, G. Barrera, R. Cavalli, Glutathione bioresponsive cyclodextrin nanosponges, Chempluschem 81 (2016) 439–443.

[32] R.M. Fontana, N. Milano, L. Barbara, A.D. Vincenzo, G. Gallo, P.L. Meo, Cyclodextrin- calixarene nanosponges as potential platforms for pH-dependent delivery of tetracycline, ChemistrySelect 4 (2019) 9743–9747.

[33] X. Wang, X. Wang, S. Jin, N. Muhammad, Z. Guo, Stimuli-responsive therapeutic metallodrugs, Chem. Rev. 119 (2019) 1138–1192.

[34] N. Traverso, R. Ricciarelli, M. Nitti, B. Marengo, A.L. Furfaro, M.A. Pronzato, et al., Role of glutathione in cancer progression and chemoresistance, 2013, Oxid. Med. Cell. Longev. (2013), 972913.

[35] M. Argenziano, C. Lombardi, B. Ferrara, F. Trotta, F. Caldera, M. Blangetti, Glutathione/pH- responsive nanosponges enhance strigolactone delivery to prostate cancer cells, Oncotarget 9 (2018) 35813–35829.

[36] Y.J. Pan, Y.Y. Chen, D.R. Wang, C. Wei, J. Guo, D.R. Lu, et al., Redox/pH dual stimuli- responsive biodegradable nanohydrogels with varying responses to dithiothreitol and glutathione for controlled drug release, Biomaterials 33 (2012) 6570–6579.

[37] W. Tang, S.C. Ng, Facile synthesis of mono-6-amino-6-deoxy-α-,β-,γ-cyclodextrin hydrochlorides for molecular recognition, chiral separation and drug delivery, Nat. Protoc. 3 (4) (2008) 691–697.

[38] M.G. Hemingway, R.B. Gupta, D.J. Elton, Hydrogel nanopowder production by inverse- miniemulsion polymerization and supercritical drying, Ind. Eng. Chem. Res. 49 (2010) 10094–10099.

[39] W. Chen, P. Zhong, F. Meng, R. Cheng, C. Deng, J. Feijen, et al., Redox and pH-responsive degradable micelles for dually activated intracellular anticancer drug release, J. Contr. Release 169 (2013) 171–179.

[40] Y. Gao, S. Zong, Y. Huang, N. Yang, H. Wen, J. Jiang, et al., Preparation and properties of a highly elastic galactomannan-poly(acrylamide-N,N-bis(acryloyl) cysteamine) hydrogel with reductive stimuli-responsive degradable properties, Carbohydr. Polym. 231 (2020), 115690.

[41] Y. Guo, S. Guo, J. Ren, Y. Zhai, S. Dong, E. Wang, Cyclodextrin functionalized graphene nanosheets with high supramolecular recognition capability: synthesis and host guest inclusion for enhanced electrochemical performance, ACS Nano 4 (2010) 4001–4010.

[42] S. Wang, Y. Hou, S. Zhang, J. Li, Q. Chen, M. Yu, et al., Sustained antibacterial activity of berberine hydrochloride loaded supramolecular organoclay networks with hydrogen-bonding junctions, J. Mater. Chem. B 6 (2018) 4972–4984.

[43] P. Liu, R. Zhang, M. Pei, Design of pH/reduction dual-responsive nanoparticles as drug delivery system for DOX: modulating controlled release behavior with bimodal drug-loading, Colloids Surf. B Biointerfaces 160 (2017) 455–461.

[44] C. Shi, S. Zhong, Y. Sun, L. Xu, S. He, Y. Dou, et al., Sonochemical preparation of folic acid-decorated reductive-responsive ε-poly-L-lysine-based microcapsules for targeted drug delivery and reductive-triggered release, Mater. Sci. Eng. C 106 (2020), 110251.

[45] B. Rybtchinski, Adaptive supramolecular nanomaterials based on strong noncovalent interactions, ACS Nano 5 (2011) 6791–6818.

[46] L.F. Scatena, M.G. Brown, G.L. Richmond, Water at hydrophobic surfaces: weak hydrogen bonding and strong orientation effects, Science 292 (2001) 908–912.

[47] T.R. Thatiparti, A.J. Shoffstall, H.A. von Recum, Cyclodextrin-based device coatings for affinity-based release of antibiotics, Biomaterials 31 (2010) 2335–2347.

[48] G. Das, A. Nicastri, M.L. Coluccio, F. Gentile, P. Candeloro, G. Cojoc, et al., FT-IR, Raman, RRS measurements and DFT calculation for doxorubicin, Microsc. Res. Tech. 73 (2010) 991–995.

[49] W. Hu, A. Mao, P. Wong, A. Larsen, P.J. Yazaki, J.Y.C. Wong, et al., Characterization of DSPE-peg2000 and its complex with doxorubicin using NMR spectroscopy and molecular dynamics, Bioconjugate Chem. 28 (2017) 1777–1790.

[50] P. Singh, X. Ren, T. Guo, L. Wu, S. Shakya, Y. He, C. Wang, A. Maharjan, V. Singh, J. Zhang, Biofunctionalization of β-cyclodextrin nanosponges using cholesterol, Carbohydr. Polym. 190 (2018) 23–30.

[51] M. Yu, L. Pan, L. Sun, J. Li, J. Shang, S. Zhang, et al., Supramolecular assemblies constructed from β-cyclodextrin-modified montmorillonite nanosheets as carriers for 5-fluorouracil, J. Mater. Chem. B 3 (2015) 9043–9052.

[52] S.N. Zhao, L.V. Minh, N. Li, V.M. Garamus, U.A. Handge, J.W. Liu, et al., Doxorubicin hydrochloride-oleic acid conjugate loaded nanostructured lipid carriers for tumor specific drug release, Colloids Surf. B Biointerfaces 145 (2016) 95–103.

[53] D. Ren, P. Chen, P. Zheng, Z. Xu, pH/redox dual response nanoparticles with poly-γ-glutamic acid for enhanced intracellular drug delivery, Colloid. Surface. 577 (2019) 412–420.

[54] M. Kanamala, W.R. Wilson, M. Yang, B.D. Palmer, Z. Wu, Mechanisms and biomaterials in pH-responsive tumour targeted drug delivery: a review, Biomaterials 85 (2016) 152–167.

[55] H.S. Yoo, T.G. Park, Folate receptor targeted biodegradable polymeric doxorubicin micelles, J. Contr. Release 96 (2004) 273–283.

[56] W. Zhang, Y. Li, L. Liu, Q. Sun, X. Shuai, W. Zhu, et al., Amphiphilic toothbrushlike copolymers based on poly(ethylene glycol) and poly(ε-caprolactone) as drug carriers with enhanced properties, Biomacromolecules 11 (2010) 1331–1338.

[57] R. Wei, L. Cheng, M. Zheng, R. Cheng, F. Meng, C. Deng, et al., Reduction-responsive disassemblable core-cross-linked micelles based on poly (ethyleneglycol)-b-poly(N-2- hydroxypropylmethacrylamide)-lipoic acid conjugates for triggered intracellular anticancer drug release, Biomacromolecules 13 (2012) 2429–2438.